International Journal of Nanomedicine

Dovepress
Taylor & Francis Group

Open Access Full Text Article

ORIGINAL RESEARCH

Multi-Focused Acoustic Radiation Force Impulse Modulation of Murine Hepatic Xenografts Enhances Nanoscale DOX@Lip Delivery and Therapeutic Effect

Size Wu, Chengfang Wang

Department of Ultrasound, The First Affiliated Hospital of Hainan Medical University, Haikou, Hainan, People's Republic of China

Correspondence: Size Wu, Department of Ultrasound, The First Affiliated Hospital of Hainan Medical University, No. 31, Longhua Road, Haikou, Hainan, 570102, People's Republic of China, Email wsz074@aliyun.com

Purpose: To investigate whether multi-focused acoustic radiation force impulse (MF-ARFI) applied to murine xenograft liver tumors prior to intravenous administration of doxorubicin-loaded PEGylated liposomes (DOX@Lip) can enhance drug delivery efficiency through modulating the enhanced permeation and retention effect of the tumor, reduce side effects, and improve antitumor effect.

Materials and Methods: DOX@Lip and tumor-mimetic matrices were synthesized and characterized. Huh-7 cells and DOX@Lip were exposed to MF-ARFI and observed. MF-ARFI was applied to both tumor-mimetic matrices and saline with DOX@Lip to assess displacement effects. Subsequently, murine xenograft models were established and underwent MF-ARFI preconditioning before DOX@Lip injection. Tumor volume dynamics and body weight changes were longitudinally monitored. Terminal assessments included histopathology (H&E), apoptosis (TUNEL), and molecular profiling (BCL-2 and BAX by Western blot) of tumors and major organs.

Results: There was no significant difference in the live/dead cell staining results between the Huh7 cells with and without MF-ARFI. There was no significant difference in cell apoptosis rates of Huh7 cells between DOX@Lip and DOX@Lip+MF-ARFI. MF-ARFI exposure induced measurable displacement of DOX@Lip in both tumor-mimetic matrices and saline. Mice receiving combined DOX@Lip and MF-ARFI treatment exhibited significantly attenuated tumor growth ($p<0.05$) and slight weight loss, which were significantly different from DOX and DOX+MF-ARFI treatments. Cardiac histopathology revealed no significant differences in myocardial toxicity between DOX@Lip and DOX@Lip+MF-ARFI groups relative to PBS controls. Conversely, tumors from the DOX@Lip+MF-ARFI group demonstrated distinct histopathological alterations compared to other groups. TUNEL staining results indicated a relatively higher level of cell apoptosis in mice treated with DOX@Lip+MF-ARFI. Molecular analyses showed MF-ARFI pretreatment significantly reduced BCL-2 expression ($p<0.05$) while elevating the BAX/BCL-2 ratio versus DOX@Lip monotherapy.

Conclusion: Preconditioning xenograft tumors with MF-ARFI prior to DOX@Lip administration faciliates DOX@Lip delivery and significantly enhances antitumor effect while reducing cardiotoxicity. This combinatorial strategy demonstrates translational potential for optimizing liposomal chemotherapeutic delivery and effect.

Plain language Summary: Doxorubicin (DOX) can be used for the therapy of some liver cancers ineligible for surgery. However, DOX has severe side effects in high concentration. Using liposomes to encapsulate DOX to form nanoscale DOX@Lip can control the release of DOX in the blood circulation and reduce side effects. DOX@Lip can pass the tumor capillary and accumulate in the tumor stroma and release sustainably. However, its release efficiency can be impacted by the tumor stroma status. If the tumor stroma becomes stasis due to necrotic tumor and other cellular debris after previous treatments, the subsequently administrated drug will be difficult to pass the capillaries to accumulate in the tumor stroma. Multi-focused acoustic radiation force impulse (MF-ARFI) is a kind of low-intensity ultrasound, with it irradiation of liver tumor, the structures of tumor stroma can occur push, pull, and displacement, facilitating the drug leak out the capillaries, promoting the waste substances in the stroma moving away. Therefore, using MF-ARFI before nanoscale drug administration can facilitate the drug delivery and distribution in the tumor. The results of this study showed that using MF-ARFI irradiated xenograft liver tumor of mice followed by intravenous infusion of DOX@Lip significantly enhanced anti-cancer effect and reduce side effects.

Received: 7 March 2025
Accepted: 21 May 2025
Published: 12 June 2025

Keywords: liver cancer, doxorubicin, liposomes, drug delivery, xenograft tumor, acoustic radiation force impulse, enhanced permeation and retention effect

Introduction

Hepatocellular carcinoma (HCC), a predominant form of liver cancer, represents a major global health challenge with high mortality rates.[1] Early-stage HCC can be effectively managed with treatments such as tumor resection or ablation, leading to better prognoses. However, a substantial number of patients present with unresectable HCC, and liver transplantation remains inaccessible due to donor shortages or comorbidities. While locoregional control, chemotherapy, radioactive seed implantation therapy, immunotherapy, and neoadjuvant chemotherapy are crucial treatments for unresectable HCC patients, their efficacy is often limited by liver function impairment or suboptimal response rates.[1] Multikinase inhibitors like sorafenib and lenvatinib have demonstrated modest improvements in survival for patients with unresectable HCC but are hindered by significant side effects.[1,2] Immunotherapy has revolutionized the approach to advanced-stage HCC management, but the overall survival has not been enhanced.[2] The current standard of care for unresectable HCC involves a combination of various treatment modalities. Enhancing the preparation and delivery of conventional anticancer drugs is a critical strategy for improving therapeutic outcomes.

Doxorubicin (DOX), a cornerstone anthracycline chemotherapeutic, exhibits dose-dependent cardiotoxicity that restricts its clinical utility. Lipid nanoparticles, particularly polyethylene glycol modified (PEGylated) liposomal formulations of doxorubicin, have emerged as effective carriers for a wide range of therapeutics. PEGylated liposomal entrapment of DOX can significantly mitigate systemic and cardiac side effects at higher doses through controlled release mechanisms.[3] Furthermore, it can enhance drug accumulation in tumors by passive tumor targeting via the enhanced permeation and retention (EPR) effect while reducing elimination by the reticulo-endothelial system.[3]

Macromolecular and nanoscale drugs are typically impermeable to cell membranes and tend to remain in the blood following intravascular administration.[4] However, in the context of malignant tumor tissues, these macromolecules can pass the abnormally leaky vascular networks to reach and accumulate at the tumor stroma to form elevated concentrations, leveraging the EPR effect.[4–6] The EPR effect has served as a fundamental concept in cancer drug delivery and the development of innovative delivery systems for over three decades.[4–6] Despite its long-standing acceptance, the EPR effect has not consistently translated into substantial improvements in therapeutic efficacy across all solid tumors in clinical settings. This discrepancy has promoted clinicians and researchers to reassess the validity of the EPR effect and acknowledge the significant heterogeneity in its manifestation within tumors.[6,7]

Unresectable HCC is often large in size and require repeated treatments. Following previous therapies, tumor necrosis may lead to the collapse of vascularity networks, disruption of the extracellular matrix, and hindered penetration of subsequent nanoscale drugs, resulting in decreased drug concentration at the tumor site, potentially leading to resistance or disease relapse.[7,8] Acoustic Radiation Force Impulse (ARFI) technology, capable of generating shear waves that induce localized displacements through cyclic tissue compression/rarefaction, can be used to manipulate tissue and cells. Multi-Focused Acoustic Radiation Force Impulse (MF-ARFI) ultrasound, specifically, can generate stronger shear waves with larger displacements.[9–11] Leveraging this technology, we hypothesize that MF-ARFI of diagnostic ultrasound system can perturb tumor tissue, modulate the tumor stroma, and alleviate stasis and elevated interstitial fluid pressure within the tumor. This approach may compress blood vessels, enhance the leakage of macromolecular and nanoscale drugs from tumor capillaries, facilitate the movement of waste substances within the tumor stroma towards adjacent tissues and venules, subsequently increase nanoscale drugs entering and accumulation in the tumor stroma through optimized EPR effect, and yield a more robust therapeutic outcome.

Materials and Methods

Materials and Animals

Dipalmitoyl phosphatidylcholine (DPPC) and distearoyl phosphatidylethanolamine-polyethylene glycol 2000 (DSPE-PEG_{2000}) were procured from Xi'an Ruixi Biotechnology Co., Ltd.(Xi'an, China); cholesterol was obtained from Shanghai

Macklin Biochemical Technology Co., Ltd. (Shanghai, China); doxorubicin hydrochloride (>98%) was sourced from Shanghai Aladdin Biochemical Technology Co., Ltd. (Shanghai, China); Dulbecco's Modified Eagle's Medium (DMEM) cell culture medium, penicillin, streptomycin, 0.25% trypsin, and Matrigel were acquired from Wuhan Procell Life Science Co., Ltd. (Wuhan, China); fetal bovine serum (FBS), Calcein-AM/PI double kit, and Annexin V-FITC/PI apoptosis kit were purchased from Yisheng Biotechnology Co., Ltd.(Shanghai, China); Bicinchoninic acid (BCA) protein assay kit, one-step TdT-mediated dUTP Nick-End Labeling (TUNEL) apoptosis assay Kit, radioimmunoprecipitation assay (RIPA) lysis buffer, cell counting kit-8 (CCK-8), 4',6-diamidino-2-phenylindole (DAPI), Cyanine5.5 amine, β-actin mouse monoclonal antibody (Catalog number AF0003), horseradish peroxidase-labeled goat anti-mouse IgG (H+L)(Catalog number A0216), and secondary antibody dilution buffer were obtained from Beyotime Biotechnology (Nantong, China); BCL-2 (Catalog number 68103-1-1Ig) and BAX (Catalog number 60267-1-Ig) monoclonal antibodies were purchased from Proteintech Group, Inc (Wuhan, China); isoflurane was procured from Shenzhen Ruiwode Lift Technology Co., Ltd.(Shenzhen, China); chloroform and pelltobarbitalum natrium were provided by the central laboratory of Hainan Medical University; hydrogel, collagen calcium phosphate, sodium chloride, agarose, agar, methyl cellulose, and hyaluronic acid were purchased from Shanghai Aladdin Bio-Chem Technology Co., Ltd (Shanghai, China); human breast epithelial cells MCF 10A and hepatocellular carcinoma cells Huh-7 were provided by the Chinese Academy of Sciences Cell Bank (Shanghai, China); BALB/c nude mice were purchased from the Guangdong Medical Experimental Animal Center (Foshan, China).

Preparation of DOX@Lip

PEGylated liposomes were employed to load the drug DOX, aiming to prolong circulation, reduce side effects, enhance drug accumulation in the tumor, and improve the anticancer effect. The preparation of drug-loaded PEGylated liposomes followed a protocol adapted from a previously established method with minor modifications.[12] In summary, 40 mg DPPC, 5 mg cholesterol, and 5 mg DSPE-PEG_{2000} were dissolved in 10 mL chloroform to create a solution, which was then rotary evaporated in a rotary evaporator (Heidolph Hei-VAP Core ML G3, Germany) at 40°C to form a thin film. The film was hydrated with 4 mL of 250 mM ammonium sulfate solution preheated to 50°C. Following a 4-hour dialysis period, 400 μL DOX aqueous solution (5 mg/mL) was added and incubated for an additional hour. The mixture was extruded through a lipid extruder (Avanti Polar Lipids Inc, Alabama, USA) using 400 nm and 200 nm polycarbonate membranes ten times each, followed by a 24-hour dialysis process to eliminate any unloaded DOX, resulting in the formation of DOX-loaded PEGylated liposomes suspension (DOX@Lip). PEGylated liposomes (Lip) without drug loaded was prepared as a blank control.

Characterization of DOX@Lip

Size, Potential, and Shape of DOX@Lip

One milligram DOX@Lip was added to 100 mL PBS and gently shaken to ensure even mixing. The suspension was then diluted 5–10 times, the size and zeta potential of DOX@Lip were measured using a nanoPartica SZ-100V2 instrument (Horiba, Kyoto, Japan) at 25°C following the manufacturer's instructions. The morphology of DOX@Lip was visualized using a transmission electron microscope (HT-7800, Hitachi, Tokyo, Japan). A small volume of the suspension was placed onto a carbon-coated copper grid, allowed to sit for 10 min, excess suspension was absorbed using filter paper. The grid was subsequently negatively stained with 2% tungstic acid for 2 min, air-dried, and then imaged under various fields and modes.

Drug Encapsulation Efficiency

The UV-Visible absorption spectrum of DOX was recorded using a UV Spectrophotometer U-2900 (Hitachi, Tokyo, Japan) at 25°C. To prepare the samples, 20 mg DOX was dissolved in 10 mL deionized water and thoroughly mixed. The solution was then diluted to various concentrations for the measurements. The fluorescence values of the different DOX solution concentrations were determined, and a fluorescence value-concentration standard curve for DOX was constructed. Subsequently, 10 mg DOX@Lip was added to 10 mL PBS and mixed to create a homogeneous suspension. The DOX@Lip suspension underwent dialysis for 24 h using a 7 kDa dialysis bag. The fluorescence values before and after dialysis were measured at 480 nm (DOX). The entrapment efficiency was calculated using the formula: Entrapment efficiency = $(M / M_0) \times 100\%$

Where M is the mass of DOX in the DOX@Lip suspension after dialysis, and M_0 is the mass of DOX before dialysis.

In vitro Drug Release

Twenty mg of DOX@Lip were added to 10 mL PBS to form a uniform suspension. The suspension was then transferred into a dialysis bag with a molecular weight cutoff of 7 kDa, sealed, and immersed in a container containing 30 mL PBS. The setup was placed on a shaker and agitated at 37°C and 100 rpm. Samples were collected at 30-minute intervals, and the released DOX was quantified using a UV-visible spectrophotometer.

In vitro Cellular Studies

Cell Culture

The previously frozen liver cancer cells Huh-7 and human breast epithelial cells MCF 10A were thawed in a rapid way and incubated in DMEM medium supplemented with 10% fetal bovine serum (containing 100 U/mL penicillin and 100 μg/mL streptomycin) at 37°C in a 5% CO_2 environment.

Cytocompatibility of Liposomes

MCF 10A cells in the logarithmic growth phase were seeded in a 96-well plate at a density of 1×10^4 cells/well. The cells were incubated overnight to allow for adherence. PEGylated liposomes were then diluted in the culture medium to various concentrations (1, 10, 25, 50, 100, 250, 500 μg/mL). Subsequently, 100 μL of each sample was added to the respective wells, and the cells were further incubated for 24 h. Following incubation, 100 μL 10% CCK-8 was added to each well. The absorbance at 450 nm was measured using a microplate reader (BioTek Synergy HTX, USA), and the cell viability after treatment with different concentrations of PEGylated liposomes was calculated.

Antiproliferative Effects of DOX / DOX@Lip

Huh-7 cells in the logarithmic growth phase were seeded in a 96-well plate at a density of 1×10^4 cells/well. The cells were incubated overnight to allow for adherence. Subsequently, DOX and DOX@Lip were diluted in the culture medium to various concentrations (2, 10, 20, 50, 100 μg/mL of DOX). 100 μL of each sample was added to the respective wells, and the cells were incubated for 24 h. Following incubation, 100 μL 10% CCK-8 was added to each well. The absorbance at 450 nm was measured using a microplate reader, and the cell viability after treatment with different concentrations of DOX and DOX@Lip was calculated. Each experiment was performed in triplicate, and cell viability was calculated relative to the control group using the formula:

Cell Viability (%) = [(OD value of the experimental group - OD value of the blank control group) / (OD value of the control group - OD value of the blank control group)] × 100%.

MF-ARFI+DOX/DOX@Lip Cytotoxicity (Fluorescence Imaging)

To evaluate the impact of MF-ARFI irradiation using the Mindray Resona 7 ultrasound system with a convex transducer operating at a frequency of 1–6MHz (Figure S1), delivering no more than 720 mW/cm^2 of derated spatial-peak temporal-average intensity(710 mW/cm^2), 50% duty cycle, for 3 min in combination with DOX@Lip on cells, the following experimental protocol was implemented: Huh-7 cells were seeded in a six-well plate at a density of 2×10^5 cells/mL and incubated in a 37°C, 5% CO_2 incubator until reaching 80–90% confluence. The cells were irradiated with MF-ARFI from the bottom of the plate. Subsequently, 2 mL DOX solution (10 μg/mL) or DOX@Lip suspension (containing 10 μg/mL DOX) was added, and the cells were incubated for 24 h. Following incubation, the culture medium was removed, and the wells were washed three times with PBS. The cells were treated with 500 μL 0.25% trypsin, centrifuged, and resuspended in 100 μL Calcein-AM/PI buffer. The cells were then stained with a mixture of Calcein-AM (2 μM) and Propidium Iodide (PI) (4.5 μM) for 15 min to distinguish between live and dead cells. The live and dead cells were visualized using an inverted fluorescence microscope (Olympus, Tokyo, Japan). Images were captured, saved on a computer, and subsequently analyzed using Image J 1.53b software.

Apoptosis Analysis of MF-ARFI + DOX/DOX@Lip (Flow Cytometry)

Huh-7 cells were seeded in a six-well plate at a density of 2×10^5 cells/mL and incubated at 37°C with 5% CO_2 to allow the cells to adhere and reach 80%-90% confluence. The experimental groups received MF-ARFI irradiation, followed by the addition of either 2 mL DOX solution (10 μg/mL) or DOX@Lip suspension (equivalent to 10 μg/mL DOX) for a 24-h

incubation. After 24 h, the culture medium was aspirated, and the cells were washed three times with PBS. Subsequently, the cells were treated with 500 μL 0.25% trypsin solution without EDTA, followed by centrifugation. The cell pellet was washed twice with PBS, centrifuged at 300 g at 4°C for 5 min. The PBS was removed, and the cells were resuspended in 100 μL of 1×Binding Buffer. Annexin V-FITC (5 μL) and PI Staining Solution (10 μL) were added, gently mixed, and incubated in the dark at room temperature for 15 min. Following incubation, 400 μL of 1×Binding Buffer was added, thoroughly mixed, and the samples were kept on ice. Cell apoptosis was analyzed using flow cytometry (BD Biosciences, Franklin Lakes, NJ, USA).

Displacement Analysis of DOX@Lip in the Tumor-Mimetic Matrix Post-MF-ARFI

Tumor-Mimetic Matrix Preparation

Tumor-like matrices were created using materials simulating the biochemical compositions of tumors, based on previous studies.[13–16] The specific ingredients and preparation methods are detailed in the supplementary materials (S2).

DOX@Lip Displacement in the Tumor-Mimetic Matrices Post-MF-ARFI

The prepared semi-solid gels (Tumor-mimetic Matrices 1, 2, and 3) were placed at the bottom of plastic containers. A small amount of Cy5.5-labeled DOX@Lip was then placed on each gel. The container was secured on a support rack with clamps, and an ultrasound transducer (1–6MHz) with sufficient coupling gel was positioned at the bottom of a larger container, ensuring direct contact without air interface. The transducer was adjusted to focus the MF-ARFI on the region of the tumor-mimetic matrix containing Cy5.5-labeled DOX@Lip. The experimental procedure involved initiating the conventional mode of ultrasound scanning, followed by activating the MF-ARFI. The dynamic changes were observed and representative images were captured within 1, 3, and 5 min, respectively.

DOX@Lip Displacement in Saline Post-MF-ARFI

A plastic container containing 20 mL 0.9% sodium chloride solution and Cy5.5-labeled DOX@Lip at the bottom was positioned in the central region of a larger plastic container filled with deionized water. The setup was secured on a supporting rack with clamps and accessories. A convex transducer (1–6MHz) with adequate coupling gel was placed at the bottom of the larger container, ensuring there were no air interface between the transducer and the container. The Cy5.5-labeled DOX@Lip was situated in the central region of the acoustic wave generated by the transducer in the container with the saline solution. MF-ARFI was then activated for durations of 1, 3, and 5 min, and the ensuing dynamic changes were observed and representative images were saved.

In vivo Therapeutic Evaluation

Xenograft Tumor Models

The animal experiments were approved by the Ethics Committee of Hainan Medical University (HYLL-2022-071). All procedures described in this study adhered to the guidelines for animal care and use at Hainan Medical University and followed the ARRIVE guidelines (Animal Research: Reporting of In Vivo Experiments). Twenty female BALB/c SPF nude mice were housed in an animal facility with environmental conditions set at 25°C, 50% relative humidity, and a 12-h light/dark cycle. Each cage accommodated 5 mice, ensuring they had access to sufficient food and water. The animals were monitored every other day for behavior, fur condition, and weight changes. All mice were used for establishing HCC tumor models. These mice weighed between 16 to 18 grams and were 4 weeks old. HCC cells Huh-7 were cultured, harvested, and suspended in PBS to a total volume of 2 mL. Subsequently, 2 mL Matrigel was added and thoroughly mixed to create a 4 mL suspension. Approximately 4×10^6 cells in 200 μL of the suspension were subcutaneously injected into the anterior region of the right hind leg of each mouse.

Treatment Protocol

Eighteen out of the 20 tumor-bearing nude mice were randomly divided into 6 groups and intravenously administered with PBS, DOX (5 mg/kg), or DOX@Lip (equivalent to 5 mg/kg DOX) with a 48-h interval between treatments. Starting from the second treatment, MF-ARFI was used to irradiate the tumor before injection (3 min, 50% duty cycle). Throughout the treatment period, the tumor size and body weight of the mice were measured every 2 days. Tumor volumes were calculated using the formula: $1/2 \times a^2b$ (where "a" represents the short axis and "b" denotes the long axis

of the tumor). On the 14th day, the nude mice were euthanized by intraperitoneal injection of 1% pentobarbital sodium solution (150 mg/kg). The criteria for determining animal death included loss of muscular tension leading to a collapsed state, gray skin color, absence of heartbeats and respiration, and mydriasis. The tumor, heart, liver, spleen, lung, and kidney were excised, washed with PBS, dehydrated using 10% formalin fixative, varying concentrations of ethanol, and xylene. Subsequently, the organs and tumor were embedded in liquid paraffin, sectioned, and stained with hematoxylin and eosin (H&E) and TUNEL. The histological features of the organs and tumor were observed and evaluated under a microscope, focusing on the cardiotoxicity and antitumor efficacy associated with DOX and MF-ARFI irradiation.

Apoptosis Protein Analysis (Western Blot)

The impact of DOX@Lip on tumor cell apoptosis following MF-ARFI irradiation was further investigated by conducting Western blot analysis of B-cell lymphoma 2 (BCL-2) and BCL-2-associated X (BAX) proteins in the cells. The Bax/Bcl-2 ratio was calculated. A comparison was made between the anti-tumor effects of DOX and DOX@Lip with and without MF-ARFI irradiation on the tumor, and their correlation with cell apoptosis was analyzed. Tumor tissues weighing 50 mg were minced, lysed using RIPA lysis buffer, and centrifuged to extract proteins. The protein concentrations were determined using the bicinchoninic acid method. Subsequently, the protein samples were separated by 10% sodium dodecyl sulfate-polyacrylamide gel electrophoresis (SDS-PAGE) and transferred to PVDF membranes via wet transfer at 400 mA for 30 min. The membranes were then blocked with 5% skim milk for 1 h, followed by overnight incubation with β-actin, BCL-2, and BAX antibodies at 4°C. The next day, the membranes were washed three times and incubated with horseradish peroxidase-labeled goat anti-mouse IgG (HL) at 25°C for 1 h. After washing, the membranes were developed using a chemiluminescent substrate following the manufacturer's instructions and imaged using AlphaEaseFC 4.0 (Alpha Innotech Corp). The densitometry analyses of protein bands intensity of the obtained images were analyzed using Image J 1.53b software.

Statistical Analysis

Normally distributed quantitative data determined by Shapiro–Wilk test were presented as mean ± standard deviation, while non-normally distributed quantitative data and qualitative data were expressed as counts, percentiles, and inter-quartile ranges. Statistical analysis involved the use of paired *t*-test and one-way ANOVA for normally distributed quantitative data, while qualitative data and non-normally distributed quantitative data were analyzed using the Chi-square test and Mann–Whitney *U*-test. A P-value of <0.05 (two-tailed) was considered statistically significant. Graphs and image analysis were conducted using GraphPad Prism 8.0 and Image J 1.53b software.

Results and Discussion

Synthesis and Characterization of DOX@Lip

Nanoscale DOX@Lip were successfully synthesized via thin-film dispersion and ammonium sulfate gradient loading (Figure 1). Transmission electron microscopy revealed uniform spherical vesicles with intact bilayer structures of DOX@Lip (Figures 2A and S2). Dynamic light scattering confirmed a hydrodynamic diameter of 125.33 ± 5.49 nm (Figure 2B) and near-neutral zeta potential of −0.07 ± 0.06 mV (Figure 2C), ideal for prolonged systemic circulation. The formulation achieved high drug encapsulation efficiency (EE) of 85.73 ± 4.07%. The release profile of DOX from DOX@Lip in PBS at pH 7.4 indicated a slow and sustained release pattern, with cumulative release rates of 19.64 ± 0.44% at 2 h and 29.25 ± 0.74% at 6 h (Figure 2D). This sustained release behavior suggests that DOX encapsulated within the PEGylated liposomes is released gradually, which could be advantageous in reducing the quick release of DOX in the blood at pH 7.4. This controlled release profile minimizes premature DOX leakage, potentially reducing cardiotoxicity and other toxicity while enabling passive tumor accumulation via the EPR effect.

In vitro Cytotoxicity and MF-ARFI Safety

Biocompatibility of PEGylated Liposomes

Blank PEGylated liposomes exhibited no cytotoxicity toward MCF 10A cells at concentrations up to 500 μg/mL, confirming their suitability as biocompatible drug carriers (Figure 3A). Biocompatibility and safety are paramount considerations in the development of drug formulations.

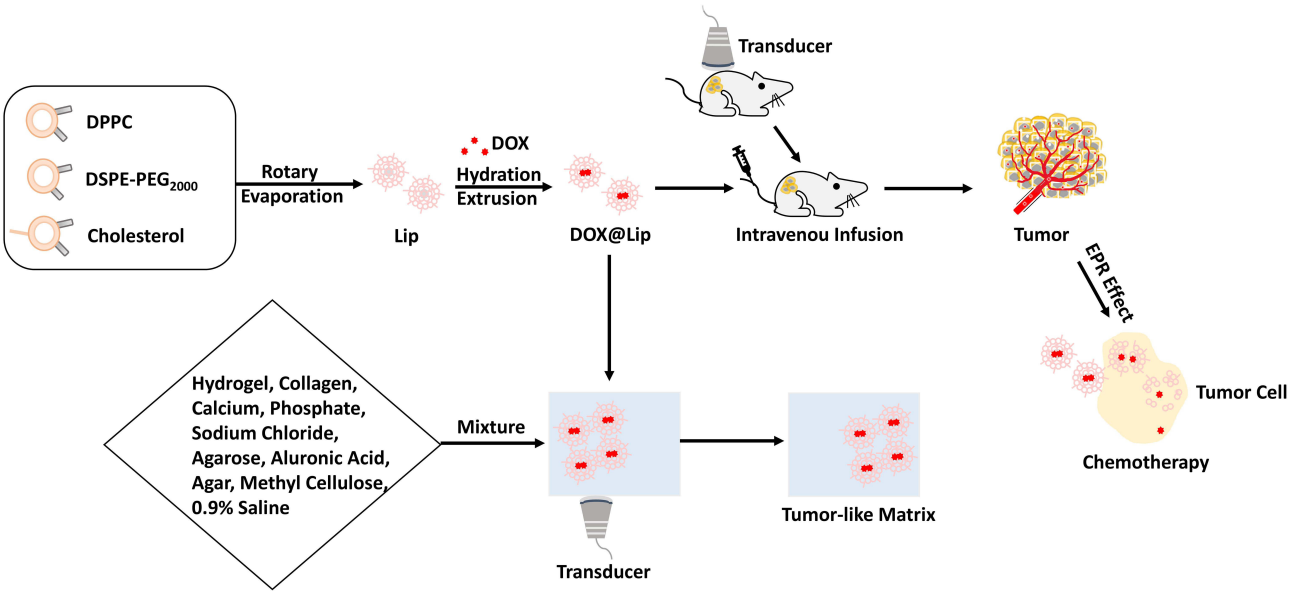

Figure 1 Schematic illustration of the preparation of DOX@Lip, tumor-mimetic matrix, and multi-focused acoustic radiation force impulse (MF-ARFI) ultrasound on DOX@Lip in the tumor-mimetic matrix, and MF-ARFI on xenograft tumor of mouse. (1) Lipids are solved in chloroform, followed by the formation of a thin film through rotary evaporation. Doxorubicin (DOX) is then loaded into the hydrophobic core of polyethyleneglycol modified (PEGylated) liposomes through hydration and extrusion, forming DOX@Lip. (2) Hydrogel, collagen, calcium phosphate, sodium chloride, agarose, aluronic acid, agar, methyl cellulose, and 0.9% physiological saline are used to make tumor-mimetic matix. (3) MF-ARFI irradiation of the tumor-mimetic matrix with prior placed DOX@Lip can cause the displacement of DOX@Lip. (4) MF-ARFI irradiates the xenograft tumor of a tumor-bearing mouse before intravenous infusion of DOX@Lip may help DOX@Lip deliver and distribute to the deeper tissues of the tumor through the enhanced permeability and retention (EPR) effect. DOX releases from the DOX@Lip and affects the cell nucleus, leading to the destruction of cancer cells.

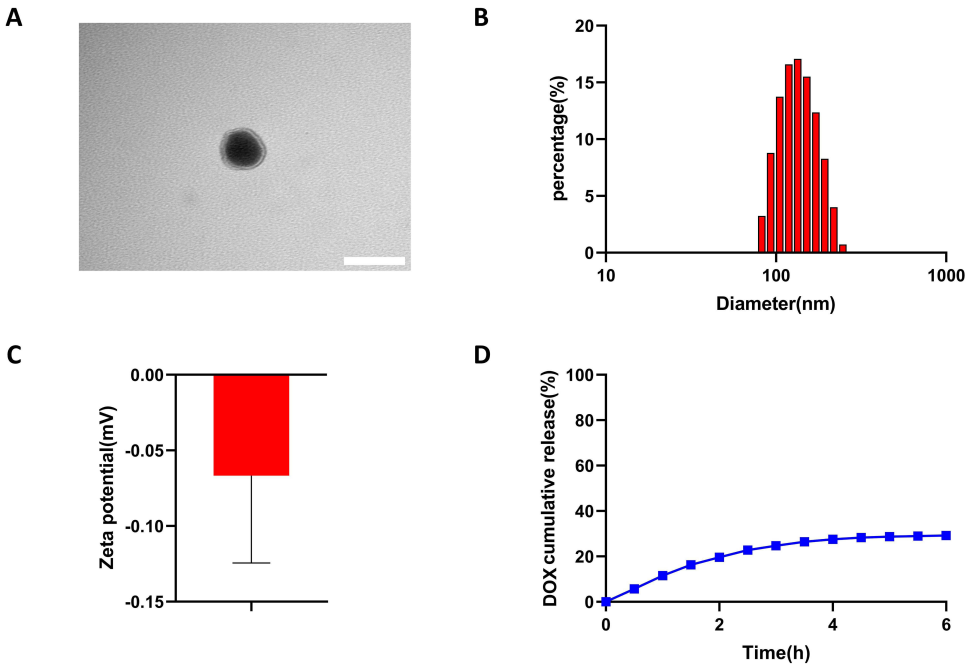

Figure 2 Characterization of DOX@Lip. (**A**) Image of DOX@Lip obtained by transmission electron microscope, a single DOX@Lip presents as a vesicular bilayer structure resembling a spherical shape; (**B**) Size of DOX@Lip is of 125.33 ± 5.49 nm; (**C**) Potential of DOX@Lip is −0.07 ± 0.06 mV; (**D**) DOX cumulative release rates of DOX@Lip are of 19.64 ± 0.44% at 2 hours and 29.25 ± 0.74% at 6 hours.

https://doi.org/10.2147/IJN.S522247

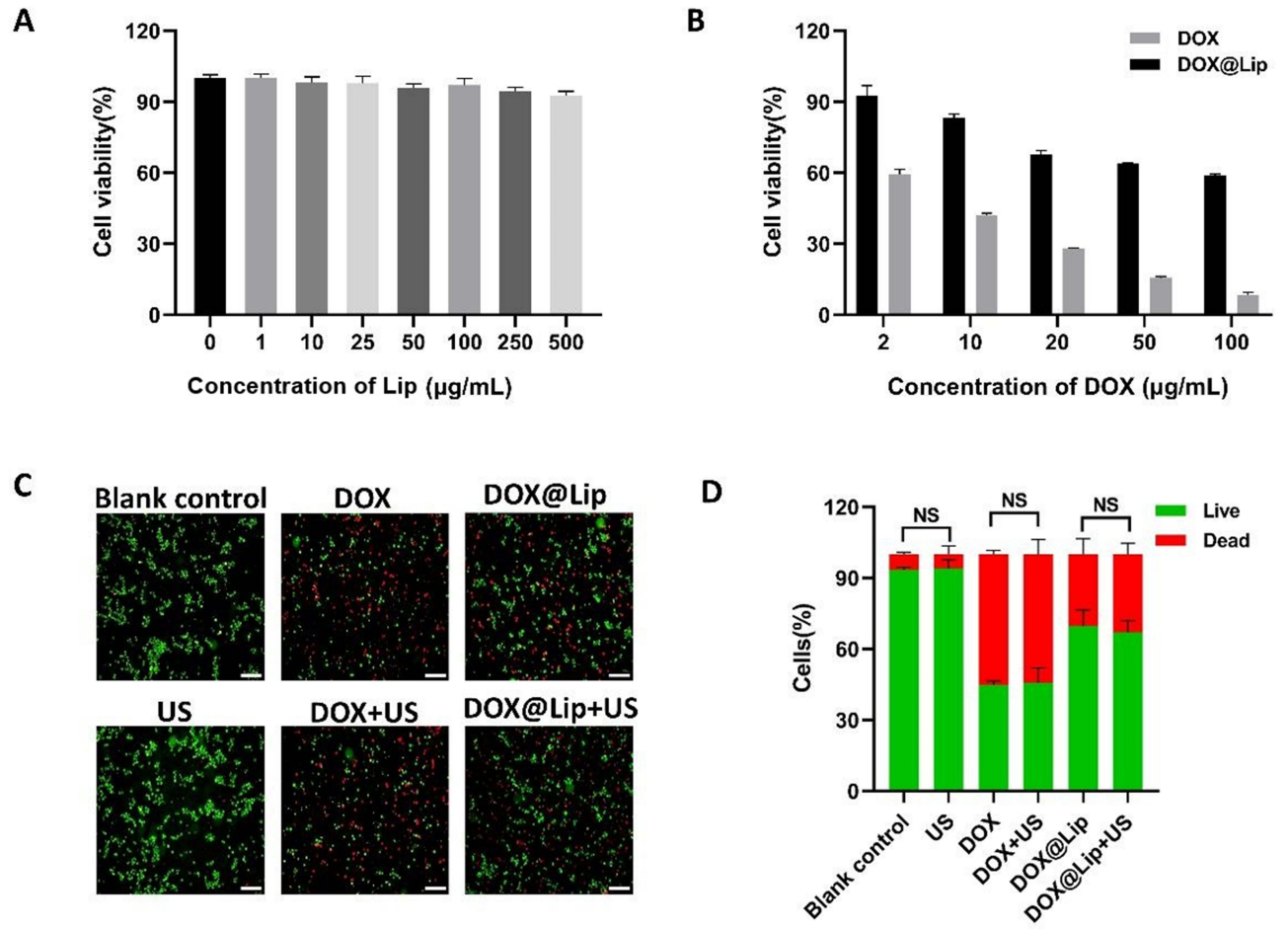

Figure 3 Cytotoxicity assay in vitro using CCK-8. (**A**) CCK-8 assay shows different concentrations of PEGylated liposomes have not demonstrated toxic effects on MCF 10A cells; (**B**) CCK-8 assay shows different concentrations of DOX@Lip exhibit varying toxicities on Huh-7 cells, with the viability of Huh-7 cells decreasing gradually as the concentration of DOX@Lip increased. DOX has more pronounced toxicity compared to DOX@Lip at equivalent doses; (**C**) AM/PI assay of DOX and DOX@Lip on Huh-7 at conditions with and without MF-ARFI exposure; (**D**) There are no significant differences in the live-dead cell staining outcomes between the cells treated with and without MF-ARFI irradiation prior to the addition of DOX or DOX@Lip. (US=MF-ARFI).

Antiproliferative Effects

Free DOX demonstrated more pronounced dose-dependent toxicity against Huh-7 cells compared to DOX@Lip at equivalent doses, whereas different concentrations of DOX@Lip exhibited varying toxicities against Huh-7 cells, with the viability of Huh-7 cells decreasing gradually as the concentration of DOX@Lip increased, showed attenuated but sustained toxicity (Figure 3B). This observation aligns with the liposomal formulation's controlled release mechanism, which delays drug availability while maintaining therapeutic efficacy.

MF-ARFI+DOX/DOX@Lip Cytotoxicity (Fluorescence Imaging)

To assess the anti-tumor effect of DOX@Lip following low intensity MF-ARFI irradiation in vitro, Huh-7 cells were stained using Calcein-AM (green fluorescence for live cells) and PI (red fluorescence for dead cells) under various experimental conditions. Live and dead cells were identified and semi-quantitatively assessed based on the staining patterns. In the experimental setup, Huh-7 cells in a six-well plate were subjected to MF-ARFI irradiation (1–6MHz, 710 mW/cm², 50% duty cycle, 3 min), followed by the addition of DOX or DOX@Lip (containing 10 μg/mL DOX) and a subsequent 24-h incubation period (Figure 3C). The results indicated no significant differences in the live/dead cell staining outcomes between the cells treated with and without MF-ARFI irradiation prior to the addition of DOX or DOX@Lip (Figure 3D), suggesting that in vitro MF-ARFI irradiation did not induce cytotoxic effects against Huh-7 cells. It is worth noting that ultrasound at a derated spatial-peak temporal-average intensity of 720 mW/cm² or lower has been validated as safe for clinical applications.[17]

Apoptosis Analysis of MF-ARFI + DOX/DOX@Lip (Flow Cytometry)

Cell apoptosis following MF-ARFI irradiation was assessed using an Annexin V-FITC/PI apoptosis kit, and performed by flow cytometry, as illustrated in Figures 4A, B and S3. The analysis revealed no significant difference in apoptosis rates between the cells irradiated with MF-ARFI and the blank control cells, suggesting that MF-ARFI irradiation did not induce substantial damage to Huh-7 cells.

The cell apoptosis rates for DOX, DOX with MF-ARFI irradiation, DOX@Lip, and DOX@Lip with MF-ARFI irradiation were determined to be 38.50 ± 3.36%, 38.47 ± 3.68%, 24.50 ± 2.52%, and 24.62 ± 1.20%, respectively. There were no significant differences in the cell apoptosis rates between DOX@Lip and DOX@Lip plus MF-ARFI irradiation. This suggests that in vitro MF-ARFI irradiation did not alter the cytotoxicity of DOX@Lip, consistent with the findings from the Calcein-AM/PI double staining. These results align with previous studies on ultrasound irradiation, despite variations in ultrasound power.[18,19] Low intensity ultrasound has been shown to promote cell apoptosis at higher power levels and inhibit cell apoptosis while increasing cell viability at lower power levels.[19,20]

MF-ARFI Enhances DOX@Lip Displacement in Tumor-Mimetic Matrix and Saline

Tumor-Mimetic Matrix Model

Tumor-mimetic matrix enabled quantitative assessment of MF-ARFI-induced DOX@Lip displacement. Cy5.5-labeled DOX@Lip exhibited 1.0 mm or so displacement within 60s of MF-ARFI exposure [Figures 5 and S4], demonstrating acoustic modulation of nanoscale DOX@Lip distribution in stroma-like environments. The extracellular matrix plays a significant role in the tumor extracellular stroma, forming the foundation of the tumor microenvironment, and exerting a substantial influence on tumor cells, impacting tumor initiation, progression, metastasis, and response to treatment. Materials such as hydrogels, collagen, agarose, and others are commonly utilized to simulate the extracellular matrix in research.[13–16] In this study, tumor-mimetic matrix models were created without the presence of cells, blood vessels, and certain biological factors typically found in the tumor stroma. While these models may not encompass all the components of a genuine tumor matrix, they exhibit some physical properties similar to those of actual tumor matrices, making them suitable for subsequent experiments.

Saline-Based Displacement of DOX@Lip

When using the conventional ultrasound scanning mode, the positions of DOX@Lips remained unchanged in both the tumor-mimetic model and the 0.9% sodium chloride solution over a period of 60s (Figure S5 and Video S1). In contrast,

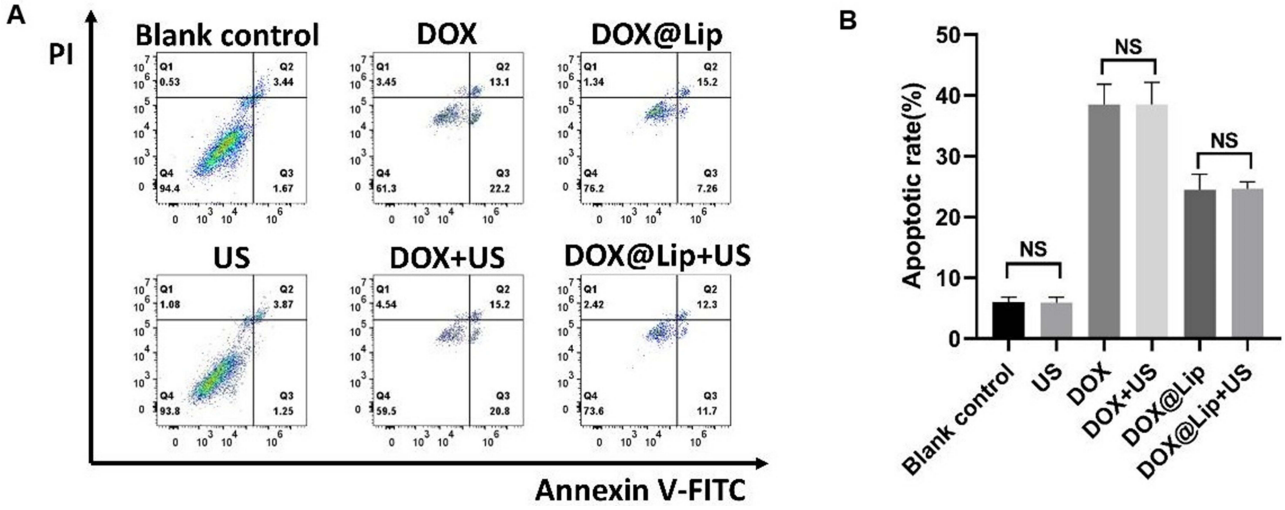

Figure 4 Cytotoxicity assay in vitro using Flow cytometry. (**A**) Flow cytometry of DOX and DOX@Lip on Huh-7 at conditions with and without MF-ARFI exposure; (**B**) The cell apoptosis rates for DOX, DOX with MF-ARFI irradiation, DOX@Lip, and DOX@Lip with MF-ARFI irradiation are of 38.50 ± 3.36%, 38.47 ± 3.68%, 24.50 ± 2.52%, and 24.62 ± 1.20%, respectively; and there were no significant differences in the cell apoptosis rates between DOX@Lip and DOX@Lip plus MF-ARFI irradiation. (US=MF-ARFI).

https://doi.org/10.2147/IJN.S522247

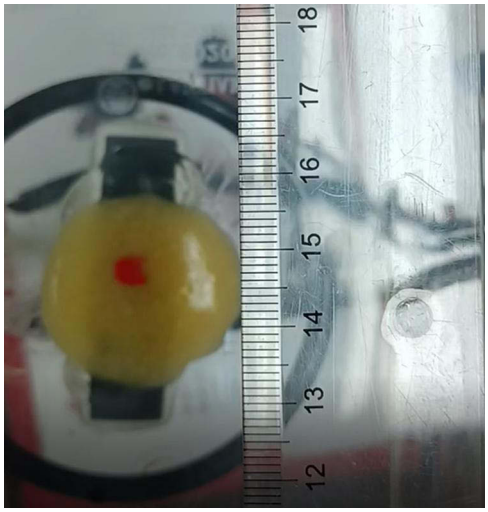

Figure 5 Effect of MF-ARFI on DOX@Lip in the tumor-mimetic matrix. Using conventional ultrasound of the diagnostic ultrasound system, Cy5.5 labeled DOX@Lip on the tumor-mimetic matrix on the plastic container remains still; using MF-ARFI of the diagnostic ultrasound system, Cy5.5 labeled DOX@Lip on the tumor-mimetic matrix on the plastic container occurs a little displacement of approximately 1 mm(visible by eye on real-time state only).

when using the MF-ARFI mode, the positions of DOX@Lips continuously changed in both the tumor-mimetic model and the 0.9% sodium chloride solution within the same timeframe. The movement pattern involved an expansion from the center to the periphery portion, transitioning from an aggregating state to a scattering state. The displacement of Cy5.5-labeled DOX@Lip in the 0.9% sodium chloride solution was approximately 6 mm within 60s [Figures 6A, B, S5 and Video S2]. This suggests that MF-ARFI can enhance nanoscale drug intratumoral distribution and facilitate the debris in the tumor stroma drainage.

Mechanistic Implications

MF-ARFI of the diagnostic ultrasound system, characterized by high acoustic energy while remaining within the human biological safety threshold(at a frequency of 1–6MHz, delivering no more than 720 mW/cm^2 of derated spatial-peak temporal-average intensity at several minutes), does not pose risks to human safety.[21] The tumor stroma, being a dissipative medium, exhibited changes in response to MF-ARFI, indicating the potential for medical diagnostic ultrasound to modulate the tumor microstructure, alter the stagnant stroma within tumors, and facilitate the delivery

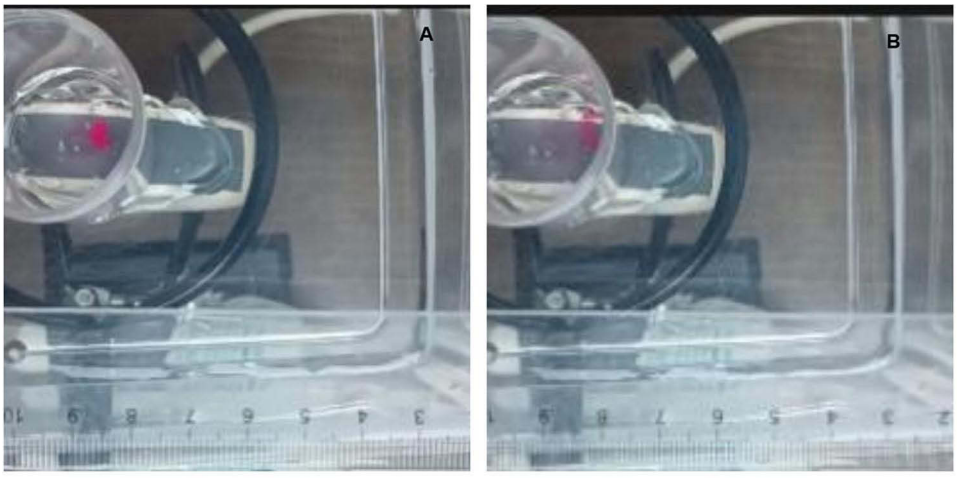

Figure 6 Effect of MF-ARFI on DOX@Lip in 0.9% sodium chloride solution. (**A**) Prior to the use of conventional ultrasound, Cy5.5 labeled DOX@Lips congregate (read region) on the bottom of the plastic container with 0.9% sodium chloride solution; (**B**) Sixty seconds exposed to MF-ARFI, Cy5.5 labeled DOX@Lips present scattering (read region) on the bottom of the plastic container with 0.9% sodium chloride solution, there is conspicuous change in shape and displacement of approximately 6 mm.

and accumulation of nanoscale drugs in tumors. Improving nanoparticle penetration of the extracellular matrix is crucial for targeted drug delivery in human tissue. Previous studies have demonstrated that low-intensity ultrasound irradiation of nanoparticles in porous mediums, such as agarose hydrogels, can significantly enhance nanoparticle penetration.[22]

Research on the effects of low intensity ultrasound on nanoparticles in gel models has been conducted. For instance, a study on collagen gel models revealed that low intensity ultrasound of ARFI caused substantial deformation of collagen gels but had no impact on the movement of nanoparticles within the gel model.[15] Another study showed that pulsed focused ultrasound applied to tumor extracellular matrix models did not increase nanoparticle penetration but enhanced nanoparticle diffusion within the tumor extracellular matrix.[16] MF-ARFI of the diagnostic ultrasound system, distinct from low intensity ultrasound used for stimuli-responsive nano-sized drug delivery systems,[23–25] provides stronger power due to the Mach cone effect of shear waves, resulting in a higher impact.[11] The push pulses generated by MF-ARFI, comprising strongly focused waves with long impulses and a center frequency of 4 MHz, induce local tissue displacement and shear wave propagation.[11] This mechanism can displace DOX@Lip in tumor-mimetic matrix models and 0.9% sodium chloride solution, facilitating drug delivery to deeper regions of the tumor and potentially enhancing drug distribution and diffusion within the tumor.

In summary, MF-ARFI of the diagnostic ultrasound system has the capability to induce the displacement of DOX@Lip in tumor-mimetic matrix models and 0.9% sodium chloride solution, potentially aiding in drug delivery to the deeper regions of tumors and improving drug distribution and diffusion within the tumor.

In vivo Therapeutic Effects of MF-ARFI+DOX/DOX@Lip

Xenograft Tumor Growth and Systemic Toxicity

To evaluate the impact of MF-ARFI of the diagnostic ultrasound system irradiation on the anticancer effect of DOX@Lip, 20 xenograft tumor models of mice had been established, 18 of them were randomly divided into 6 groups, each containing 3 mice: PBS, MF-ARFI, DOX, DOX+MF-ARFI, DOX@Lip, and DOX@Lip (equivalent to 200μL DOX)+MF-ARFI. The mice were intravenously injected with PBS, DOX, or DOX@Lip via the tail vein. The weights of the mice after treatment were 22.37±1.07g, 20.57±1.38g, 13.03±0.55g, 15.63±1.50g, 17.10±2.16g, and 18.50±1.06g, respectively [Figure 7A and Table S1]. The weight of tumor-bearing mice significantly decreased in the mice treated with DOX and DOX+MF-ARFI ($p<0.05$), while no significant decrease was observed in the mice treated with DOX@Lip and DOX@Lip+MF-ARFI ($p>0.05$). This indicates that DOX, when encapsulated in PEGylated liposomes, can effectively reduce the side effects associated with DOX treatment.

The tumor sizes in mice after treatment with PBS, MF-ARFI, DOX, DOX+MF-ARFI, DOX@Lip (equivalent to 200μL DOX), and DOX@Lip (equivalent to 200μL DOX)+MF-ARFI were 2128.43±404.61mm^3, 2312.49±820.29mm^3, 489.43 ±188.87mm^3, 515.21±147.02mm^3, 1120.37±57.45mm^3, and 449.35±86.51mm^3, respectively [Figure 7B and Table S2]. The change in tumor size between pretreatment and post-treatment for mice treated with PBS and PBS+MF-ARFI showed no significant difference (t value of 0.273, p value of 0.810). Similarly, the change in tumor size for mice treated with DOX and DOX+MF-ARFI did not significantly differ (t value of 0.040, p value of 0.972). However, there was a significant difference in tumor size change for mice treated with DOX@Lip and DOX@Lip+MF-ARFI (t value of 13.701, p value of 0.005).

The tumor inhibition rate (change in tumor size) did not significantly differ between mice treated with DOX alone and those treated with DOX+MF-ARFI (p value >0.05), suggesting that MF-ARFI did not enhance the anticancer effect of DOX treatment. However, the tumor inhibition rate in mice treated with DOX@Lip+MF-ARFI was significantly higher than that in mice treated with DOX@Lip alone ($p<0.05$) [Figure 7C and Table S2]. This indicates that MF-ARFI significantly increased the anticancer effect of DOX@Lip treatment. The rationale behind this enhancement is believed to be the ability of MF-ARFI to improve the delivery of DOX@Lip to the deeper regions of the tumor and facilitate DOX release. Although direct experimental evidence was not provided in this study, a previous study based on an animal tumor model supported the notion that ARFI could enhance the distribution of nanoparticles within the tumor stroma.[26]

Overall, MF-ARFI's shear waves (Mach cone effect) likely remodeled tumor stroma, enhancing DOX@Lip extravasation and intratumoral distribution. This aligns with prior evidence of ARFI improving nanoparticle penetration in dense matrices.

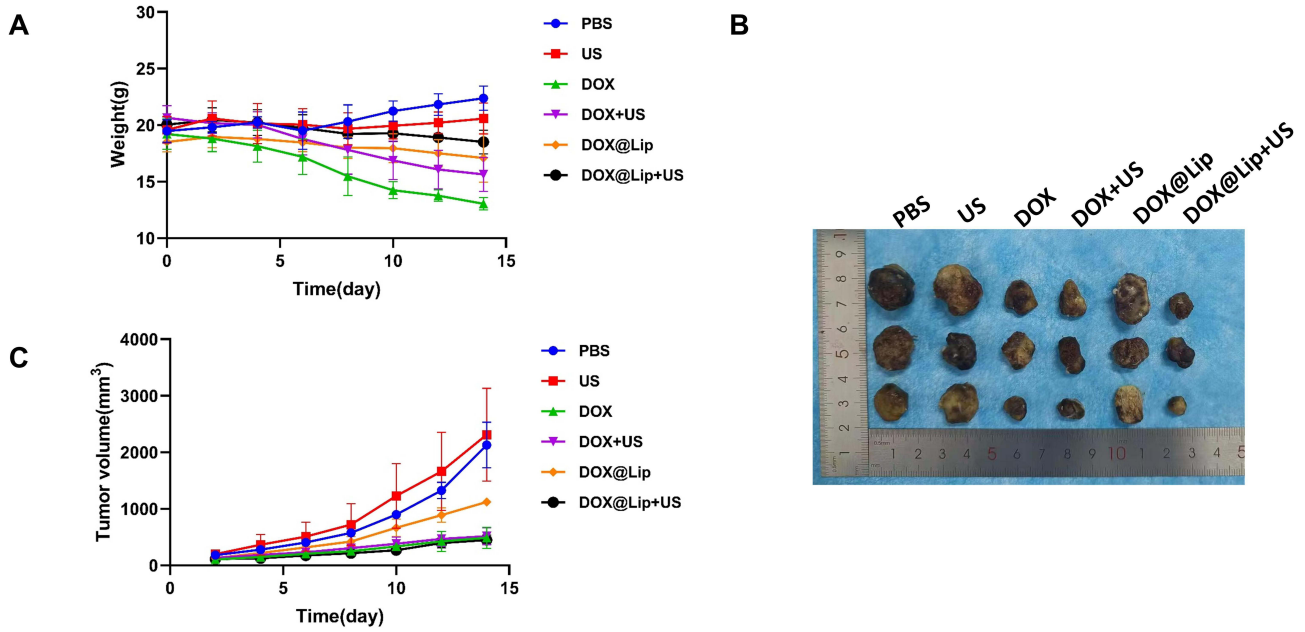

Figure 7 Anti-tumor effects of different treatments in vivo. (**A**) Weight curve of the tumor-bearing mice after different treatments in 14 days. The weight of tumor-bearing mice significantly decreases in the mice treated with DOX and DOX plus MF-ARFI irradiation ($p<0.05$), while there is no significant decreasing in the mice treated with DOX@Lip and DOX@Lip plus MF-ARFI irradiation ($p>0.05$); (**B**) Representative tumors of the tumor-bearing mice after different treatments in 14 days; (**C**) Tumor volume curve of the tumor-bearing mice after different treatments in 14 days. The change in tumor size between pretreatment and post-treatment for mice treated with PBS and PBS plus MF-ARFI irradiation shows no significant difference ($p = 0.810$); the change in tumor size for mice treated with DOX and DOX plus MF-ARFI irradiation has no significant difference ($p = 0.972$); there is a significant difference in tumor size change for mice treated with DOX@Lip and DOX@Lip plus MF-ARFI irradiation ($p = 0.005$). (US=MF-ARFI).

Histopathological and Apoptotic Analysis

H&E staining of the heart sections revealed no significant differences in the appearance, size, arrangement, nuclear shape, and cytoplasm staining intensity of cardiac cells in mice treated with DOX@Lip and those treated with DOX@Lip +MF-ARFI, compared to mice treated with PBS. This suggests that the DOX carried by DOX@Lip did not induce significant toxicity to the heart during the treatment. The antitumor effect of DOX@Lip+MF-ARFI was evident in H&E and TUNEL staining [Figures 8, 9, S7 and S8]. The H&E staining results demonstrated that tumor tissues in mice treated with DOX@Lip+MF-ARFI exhibited significant nuclear condensation, fragmentation, and dissolution compared to other treatments [Figures 8 and S7]. Additionally, the TUNEL staining results indicated a significantly higher level of cell apoptosis in mice treated with DOX@Lip+MF-ARFI [Figures 9 and S8] ($p<0.01$). Overall, MF-ARFI+DOX@Lip significantly enhanced the antitumor effect.

Apoptosis, a regulated cellular process, can be regulated by the expression of specific proteins, providing insights into the apoptotic state.[27,28] B-cell lymphoma-2 protein (BCL-2) exerts a significant anti-apoptotic effect, while BCL-2 associated X protein (BAX) can counteract BCL-2 function by forming a heterodimer. The BAX/BCL-2 ratio plays a crucial role in determining the strength of the anti-apoptotic effect.[29–32] In this study, the BCL-2 and BAX proteins in HCC cells were evaluated to investigate the regulatory impact of MF-ARFI in combination with DOX@Lip on cell apoptosis [Figures 10A and S9]. The results indicated that MF-ARFI prior to the administration of DOX@Lip significantly decreased the expression of BCL-2 ($p<0.05$) [Figure 10B], while there was no significantly change of the expression of BAX ($p>0.05$) [Figure 10C], leading to an increased BAX/BCL-2 ratio and reduced inhibition of apoptosis by BCL-2, ultimately inhibiting xenograft tumor growth.

The mechanism by which MF-ARFI of the diagnostic ultrasound system promotes the anticancer effect of DOX@Lip is believed to involve the generation of shear waves. The front of the shear wave, resembling a Mach cone moving at supersonic speed, subjects objects to a substantial amount of mechanical energy, cavitation effects, and mechanical effect.[11] MF-ARFI and the shear wave it generates can induce oscillation, compression, and rarefaction effects within the

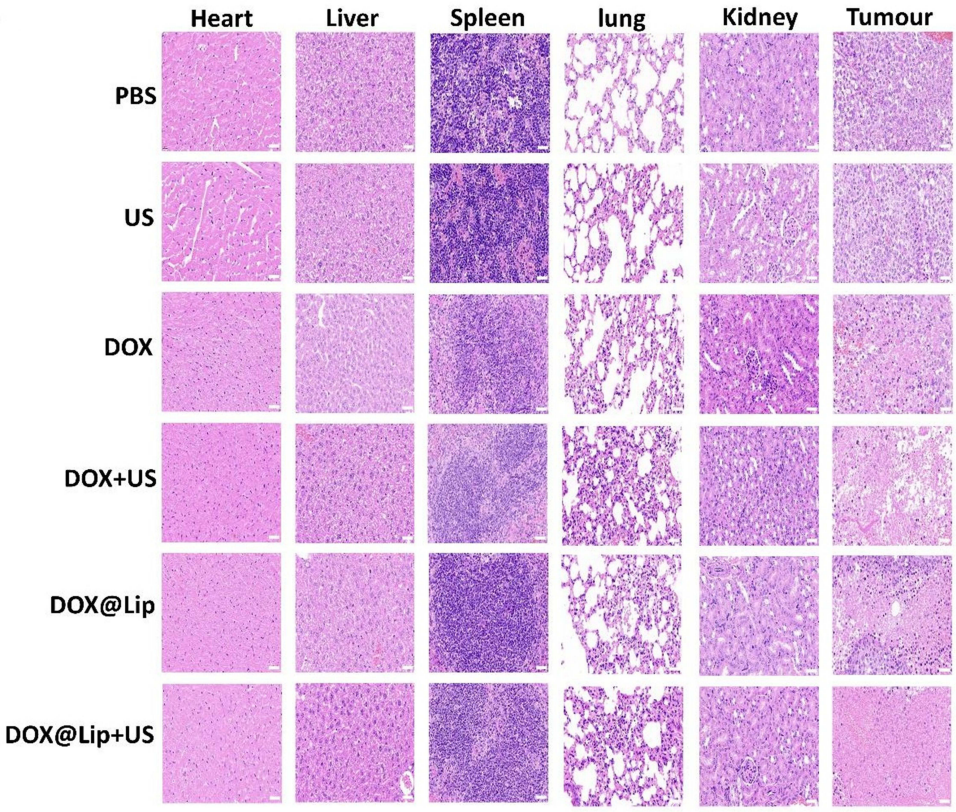

Figure 8 Anti-tumor effects of different treatments based on histology. Hematoxylin and eosin staining of the sections of tumors and visceral organs after 14 days different treatments.(US=MF-ARFI).

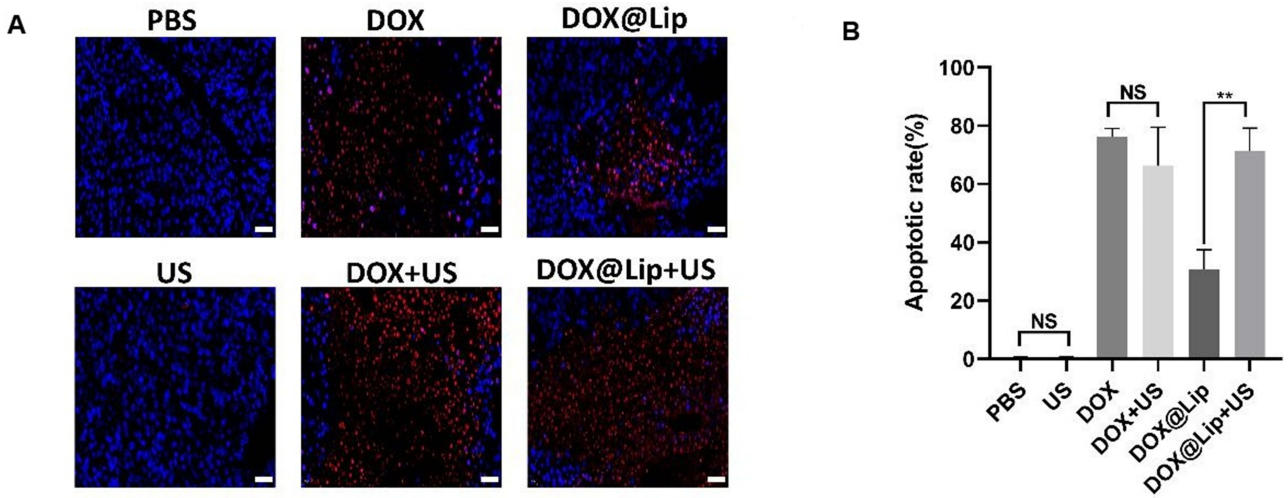

Figure 9 Anti-tumor effects of different treatments based on TUNEL. (**A**) TUNEL on cell apoptosis of tumors after 14 days different treatments; (**B**) Semi quantitative study of TUNEL on cell apoptosis of tumors after 14 days different treatments. **indicates $p<0.01$. (US=MF-ARFI).

internal structure of the tumor, leading to the displacement of internal substances. This modulation can impact the status of the tumor stroma, enhance the EPR effect of the tumor, increase the permeability of tumor microvessels, and promote the delivery, distribution, and accumulation of macromolecular drugs within the tumor. Consequently, this process enhances the anticancer effect of DOX@Lip.

https://doi.org/10.2147/IJN.S522247

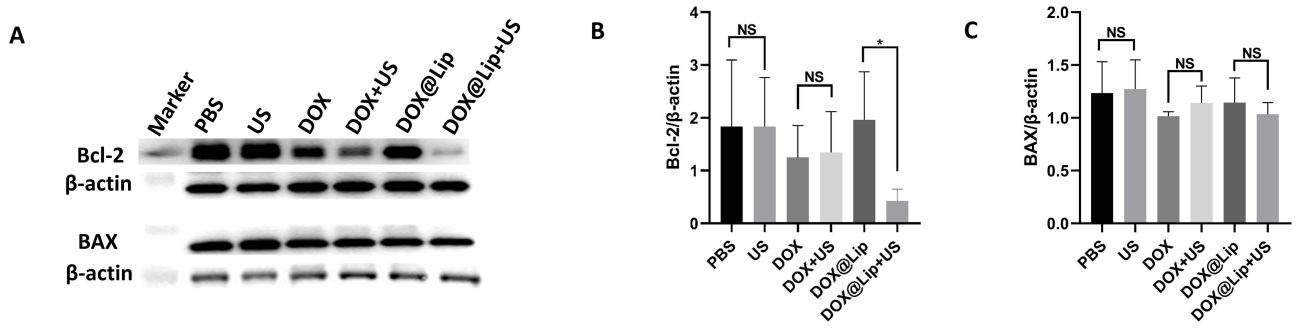

Figure 10 Western blotting analysis of the tumor. (**A**) Western blotting of BCL-2 and BAX expression of tumors after 14 days different treatments; (**B**) Semiquantitative analysis of Western blotting shows MF-ARFI irradiation prior to the administration of DOX@Lip significantly decreases the expression of BCL-2; * indicates $p<0.05$; (**C**) Semiquantitative analysis of Western blotting shows there is no significantly change of the expression of BAX ($p>0.05$). (US=MF-ARFI).

Limitations

Firstly, this study lacked of precise observation and measurement of the displacement of DOX@Lip in the tumor-mimetic matrix following MF-ARFI under controlled conditions. Secondly, displacement dynamics of DOX@Lip in tumors were inferred but not directly quantified via real-time imaging or other approach, which may have impacted the study's quality to some extent. Thirdly, small cohort size of mice (n=3/group) may limit statistical power.

Conclusion

Nano-size DOX@Lip had been synthesized, with high encapsulation efficiency. It can controlled release and get passive tumor targeting via EPR effect. MF-ARFI can cause nanoscale DOX@Lip displacement in tumor-mimetic matrix and saline, suggesting enhance DOX@Lip penetration and distribution in tumor. In vivo experiment showed MF-ARFI can mechanically (Mach cone effect) modulate xenograft tumor of mice, facilitate DOX@Lip delivery and distribute to the tumor stroma, enhance therapeutic effect, and mitigate side effects, especially the cardiotoxicity, offering a promising approach for stromal-rich, treatment-resistant tumors. MF-ARFI of diagnostic ultrasound system is within FDA (Food and Drug Administration, Center for Devices and Radiological Health, USA) standards of acoustic intensity safety thresholds (720 mW/cm²), enabling translation for unresectable hepatocellular carcinoma.

Acknowledgments

This study was supported by Hainan Province Science and Technology Special Fund No. ZDYF2023SHFZ138.

Author Contributions

All authors made a significant contribution to the work reported, whether that is in the conception, study design, execution, acquisition of data, analysis and interpretation, or in all these areas; took part in drafting, revising or critically reviewing the article; gave final approval of the version to be published; have agreed on the journal to which the article has been submitted; and agree to be accountable for all aspects of the work.

Disclosure

The authors report no conflicts of interest in this work.

References

1. Brown ZJ, Tsilimigras DI, Ruff SM, et al. Management of hepatocellular carcinoma: a review. *JAMA Surg*. 2023;158(4):410–420. doi:10.1001/jamasurg.2022.7989
2. Persano M, Rimini M, Tada T, et al. Clinical outcomes with atezolizumab plus bevacizumab or lenvatinib in patients with hepatocellular carcinoma: a multicenter real-world study. *J Cancer Res Clin Oncol*. 2023;149:5591–5602.
3. Gyöngyösi M, Lukovic D, Zlabinger K, et al. Liposomal doxorubicin attenuates cardiotoxicity via induction of interferon-related DNA damage resistance. *Cardiovasc Res*. 2020;116:970–982.
4. Lahooti B, Akwii RG, Zahra FT, et al. Targeting endothelial permeability in the EPR effect. *J Control Release*. 2023;361:212–235.

5. Wang C, Wu S. Research update on cell membrane camouflaged nanoparticles for cancer therapy. *Front Bioeng Biotechnol*. 2022;10:944518. doi:10.3389/fbioe.2022.944518
6. Maeda H. The 35th anniversary of the discovery of EPR effect: a new wave of nanomedicines for tumor-targeted drug delivery-personal remarks and future prospects. *J Pers Med*. 2021;11:229.
7. Xu M, Zhang T, Xia R, et al. Targeting the tumor stroma for cancer therapy. *Mol Cancer*. 2022;21(1):208. doi:10.1186/s12943-022-01670-1
8. Zhang R, Ma M, Dong G, et al. Increased matrix stiffness promotes tumor progression of residual hepatocellular carcinoma after insufficient heat treatment. *Cancer Sci*. 2017;108:1778–1786.
9. Nightingale K, Soo MS, Nightingale R, et al. Acoustic radiation force impulse imaging: in vivo demonstration of clinical feasibility. *Ultrasound Med Biol*. 2002;28:227–235.
10. Nightingale KR, Palmeri ML, Nightingale RW, et al. On the feasibility of remote palpation using acoustic radiation force. *J Acoust Soc Am*. 2001;110(1):625–634. doi:10.1121/1.1378344
11. Nowicki A, Dobruch-Sobczak K. Introduction to ultrasound elastography. *J Ultrason*. 2016;16(65):113–124. doi:10.15557/JoU.2016.0013
12. Wang C, Wu S. Hybrid cell membranes camouflage liposomes containing payloads to improve breast cancer chemo and photodynamic therapy. *Biomater Sci*. 2024;12(19):4980–4992. doi:10.1039/D4BM00772G
13. Ma D, Marshall JS, Wu J. Measurement of ultrasound-enhanced diffusion coefficient of nanoparticles in an agarose hydrogel. *J Acoust Soc Am*. 2018;144(6):3496. doi:10.1121/1.5083828
14. Dou Y, Fa X, Gu Y, et al. Fabrication and characterization of PVA/CS-PCL/gel multi-scale electrospun scaffold: simulating extracellular matrix for enhanced cellular infiltration and proliferation. *J Biomater Sci Polym Ed*. 2020;31(6):729–746. doi:10.1080/09205063.2020.1714534
15. Lovmo MK, Yemane PT, Bjorkoy A, et al. Effect of acoustic radiation force on displacement of nanoparticles in collagen gels. *IEEE Trans Ultrason Ferroelectr Freq Control*. 2021;68(3):416–431. doi:10.1109/TUFFC.2020.3006762
16. Einen C, Price SEN, Ulvik K, et al. Nanoparticle dynamics in composite hydrogels exposed to low-frequency focused ultrasound. *Gels*. 2023;9:771.
17. Stratmeyer ME, Greenleaf JF, Dalecki D, et al. Fetal ultrasound: mechanical effects. *J Ultrasound Med*. 2008;27(4):597–605. doi:10.7863/jum.2008.27.4.597
18. Maeda K, Shigemura K, Hayashi F, et al. Proapoptotic effect of nonthermal pulsed ultrasound on prostate cancer cells in a nude mouse model. *Prostate*. 2023;83(12):1217–1226. doi:10.1002/pros.24581
19. Maeshige N, Kitagawa K, Yamasaki S, et al. Can ultrasound irradiation be a therapeutic option for prostate cancer? *Prostate*. 2020;80(12):986–992. doi:10.1002/pros.24030
20. Hu Y, Jia Y, Wang H, et al. Low-intensity pulsed ultrasound promotes cell viability and inhibits apoptosis of H9C2 cardiomyocytes in 3D bioprinting scaffolds via PI3K-Akt and ERK1/2 pathways. *J Biomater Appl*. 2022;37:402–414.
21. Barnett SB, Ter Haar GR, Ziskin MC, et al. International recommendations and guidelines for the safe use of diagnostic ultrasound in medicine. *Ultrasound Med Biol*. 2000;26:355–366.
22. Karki A, Marshall JS, Wu J. Effect of ultrasound amplitude and frequency on nanoparticle diffusion in an agarose hydrogel. *J Acoust Soc Am*. 2022;152(1):640. doi:10.1121/10.0012972
23. Moradi Kashkooli F, Jakhmola A, Hornsby TK, et al. Ultrasound-mediated nano drug delivery for treating cancer: fundamental physics to future directions. *J Control Release*. 2023;355:552–578.
24. Li Q, Tang Z, Zhang Y, et al. Application of low-intensity ultrasound by opening blood-brain barrier for enhanced brain-targeted drug delivery. *Int J Pharm*. 2023;642:123191. doi:10.1016/j.ijpharm.2023.123191
25. Moreno-Gomez N, Athanassiadis AG, Poortinga AT, et al. Antibubbles enable tunable payload release with low-intensity ultrasound. *Adv Mater*. 2023;35(e2305296). doi:10.1002/adma.202305296
26. Afadzi M, Myhre OF, Yemane PT, et al. Effect of acoustic radiation force on the distribution of nanoparticles in solid tumors. *IEEE Trans Ultrason Ferroelectr Freq Control*. 2021;68:432–445.
27. D'Arcy MS. Cell death: a review of the major forms of apoptosis, necrosis and autophagy. *Cell Biol Int*. 2019;43(6):582–592. doi:10.1002/cbin.11137
28. Strobel T, Swanson L, Korsmeyer S, et al. BAX enhances paclitaxel-induced apoptosis through a p53-independent pathway. *Proc Natl Acad Sci U S A*. 1996;93(24):14094–14099. doi:10.1073/pnas.93.24.14094
29. Mirjolet JF, Barberi-Heyob M, Didelot C, et al. Bcl-2/Bax protein ratio predicts 5-fluorouracil sensitivity independently of p53 status. *Br J Cancer*. 2000;83(10):1380–1386. doi:10.1054/bjoc.2000.1455
30. Lopez A, Reyna DE, Gitego N, et al. Co-targeting of BAX and BCL-XL proteins broadly overcomes resistance to apoptosis in cancer. *Nat Commun*. 2022;13(1):1199. doi:10.1038/s41467-022-28741-7
31. Khodapasand E, Jafarzadeh N, Farrokhi F, et al. Is Bax/Bcl-2 ratio considered as a prognostic marker with age and tumor location in colorectal cancer?. *Iran Biomed J*. 2015;19(2):69–75. doi:10.6091/ibj.1366.2015
32. Mansour E, Abd-Rabou AA, El-Atawy MA, et al. Induction of breast cancer cell apoptosis by novel thiouracil-fused heterocyclic compounds through boosting of Bax/Bcl-2 ratio and DFT study. *Bioorg Chem*. 2024;146:107292.